Supporting Information for

Substituted SrFeO$_3$ as Robust Oxygen Sorbents for Thermochemical Air Separation: Correlating Performance with Compositional and Structural Properties

Emily Krzystowczyk,†Xijun Wang,† Jian Dou, Vasudev Haribal, Fanxing Li

Department of Chemical and Biomolecular Engineering, North Carolina State University, 911 Partners Way, Raleigh, North Carolina 27695-7905, United States
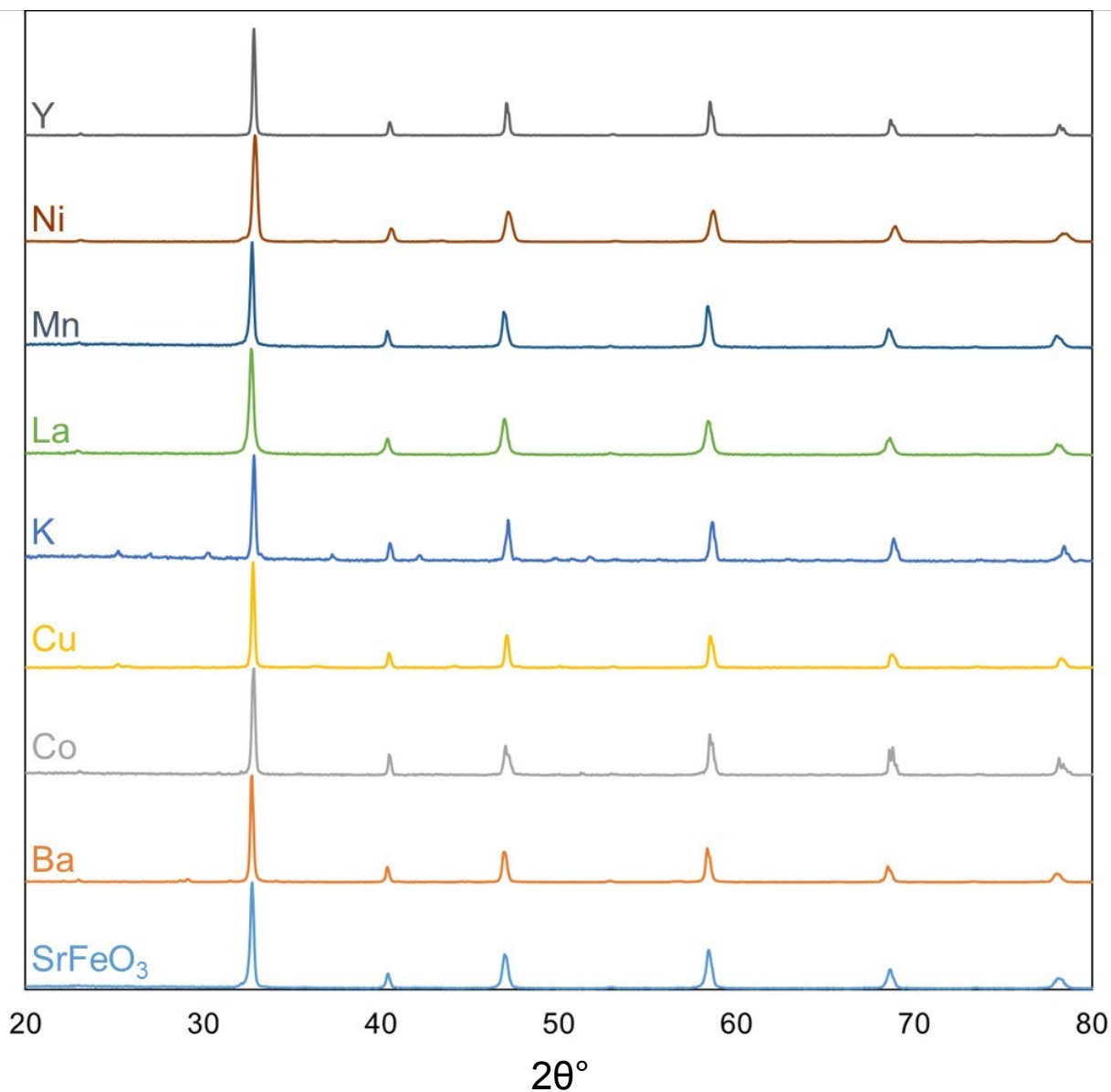
†co-first authors
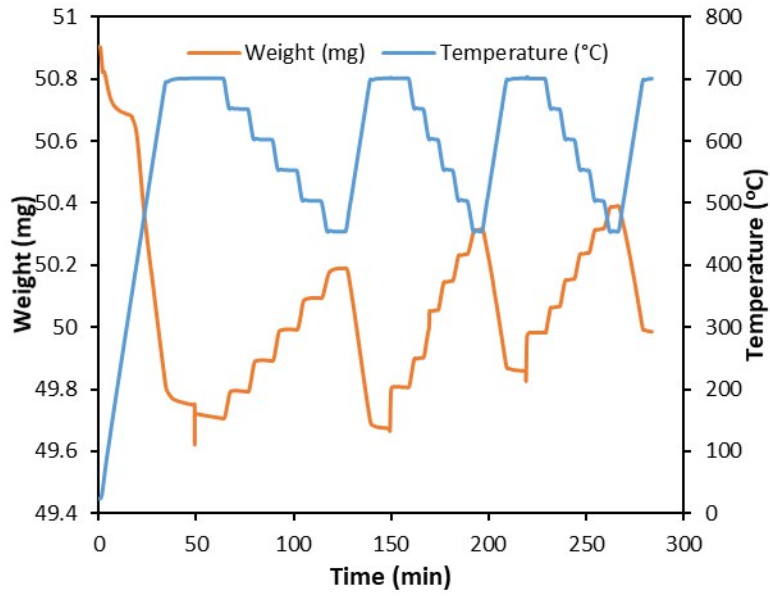
Figure S1: Example thermogravemetric curve of the Ba doped sample. Orange curve is weight in mg and blue curve is temperature in C.
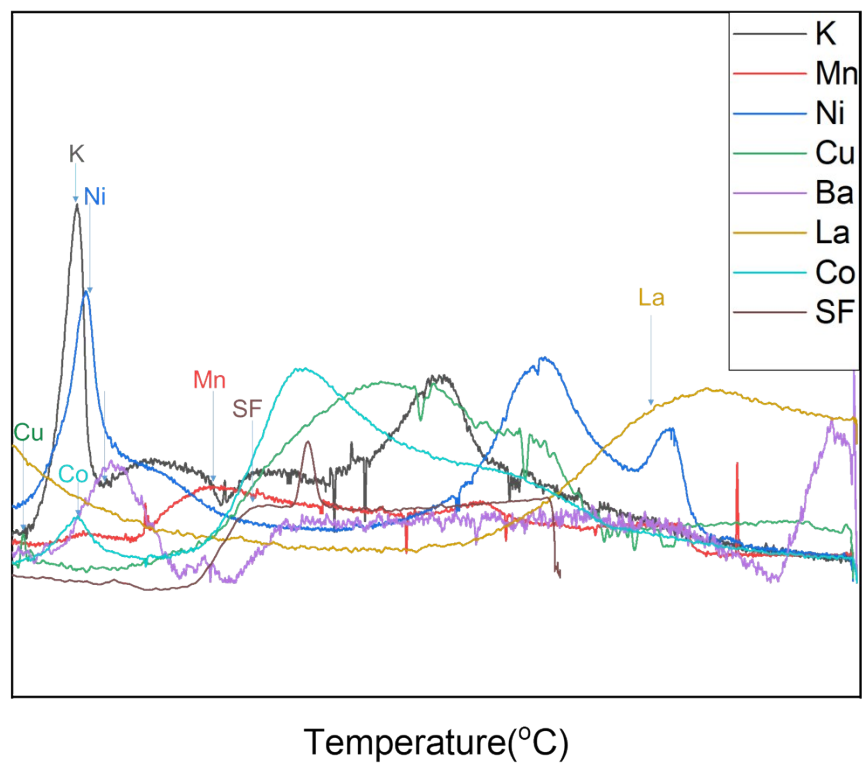
**Figure S2**: Temperature programed desorption of all tested perovskites in Ar and ramped to 1000 C.

Figure S3: XRD images of all samples tested to confirm phase.* Small amount of phase impurities appeared in K, Cu, and Ba doped samples. Their contents are estimated to be less than 3% in all cases. Possible compositions are given based on the phase diagrams (Figure S4 – S6). They are not anticipated to contribute to CLAS activities.
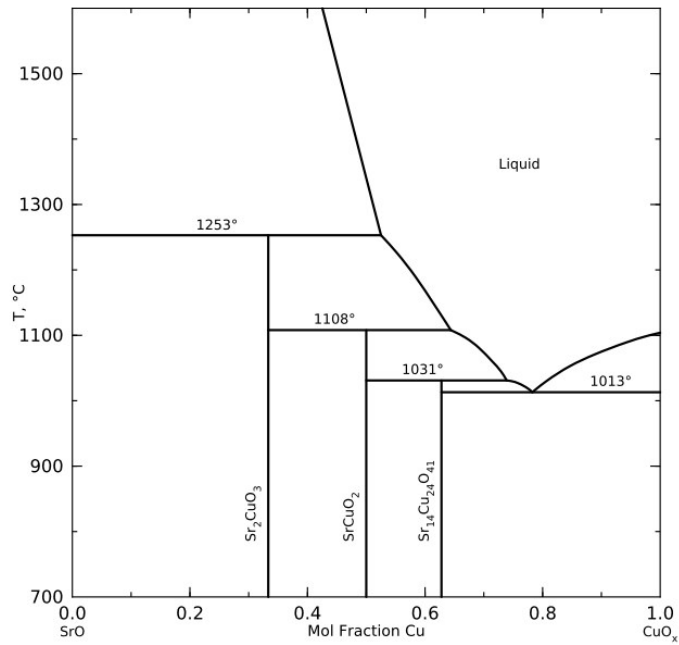
Figure S4: Phase equilibrium data of Sr-Cu-O[1] in 20% oxygen.

All potential phases at 1000 °C (our calcination temperature) Cu has an oxidation state of +2. Reduction of Cu to the +1 state is very difficult and requires temperatures higher than the scope of CLAS.
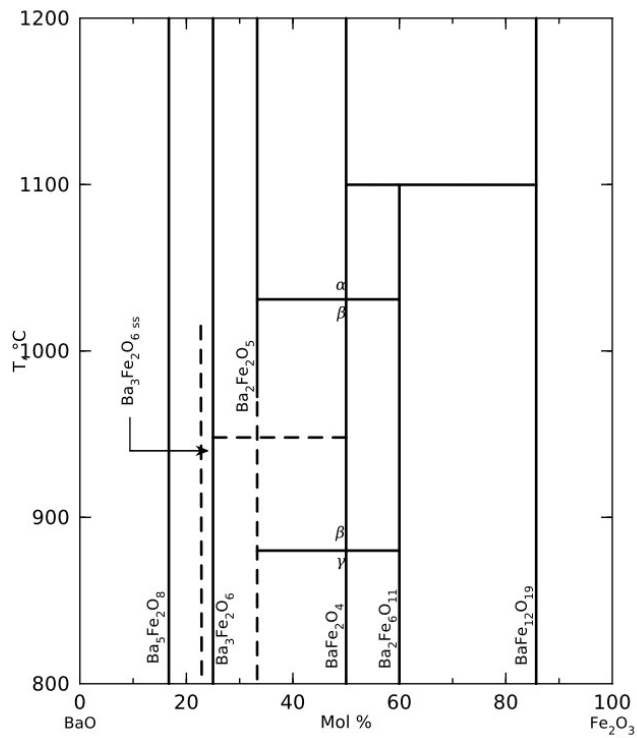
Figure S5: Phase equilibrium data of Ba-Fe-O[2] in 20% oxygen.

Possible phases at 1000 °C have Fe in a +3 state, non-reducible at CLAS relevant temperatures.
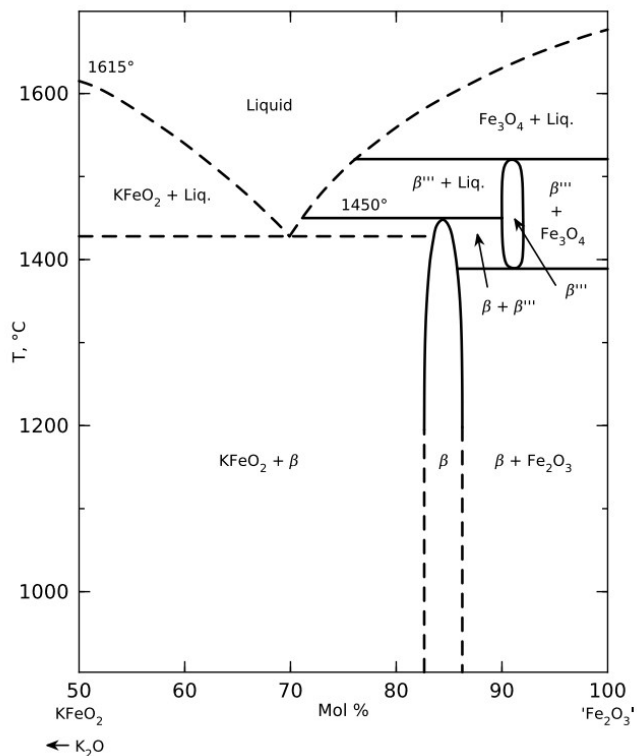
Figure S6: Phase equilibrium data of K-Fe-O in 20% air[3–5].

Table S1: 2-theta angles for the primary diffraction peak in the perovskite phase for $SrFeO_3$ and for each of the doped samples. Shifts in the peaks indicate changes in unit cell parameters.

Material	2θ
$SrFeO_3$	32.75
Ba	32.73
Co	32.85
Cu	32.8
K	32.85
La	32.72
Mn	32.75
Ni	32.9
Y	32.85
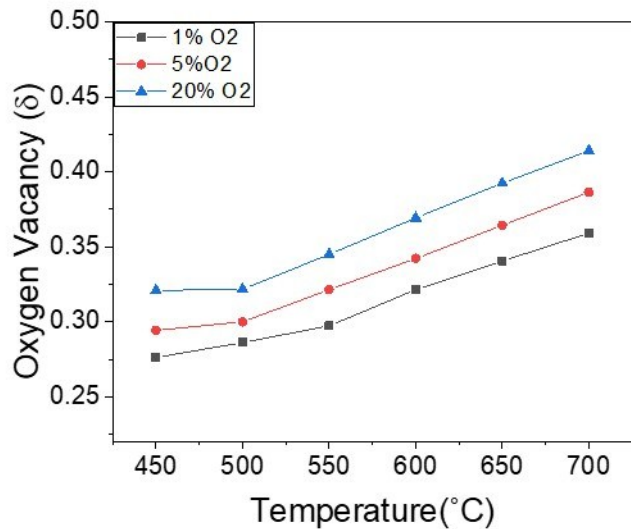
Figure S7. Oxygen vacancy (δ) of $SrFeO_{3-\delta}$ as a function of temperature and oxygen partial pressure

DFT Computational Details

First-principles simulations were performed at the DFT level implemented by the Vienna ab initio simulation package (VASP)[6] with the all-electron projector augmented wave (PAW) model[7] and Perdew-Burke-Ernzerhof (PBE) functions.[8] A kinetic energy cutoff of 450 eV was used for the plane-wave expansion of the electronic wave function. The convergence criterions of force and energy were set as 0.01 eVÅ^{-1} and 10^{-5} eV, respectively. A Gaussian smearing of 0.1 eV was applied for optimization. A $2 \times 1 \times 2$ Gamma-centered k-point grid was chosen for the brownmillerite ($Sr_8Fe_8O_{20}$) and the lattice-redefined perovskite ($Sr_8Fe_8O_{24}$) (**Figure S8**) unit cell which contains 36 and 40 atoms respectively. In our simulations the $2 \times 1 \times 1$ brownmillerite ($Sr_{16}Fe_{16}O_{40}$) and perovskite ($Sr_{16}Fe_{16}O_{48}$) supercell were used with two out of 16 Sr or Fe atoms replaced by A or B site dopant to mimic the doped materials, where A represents Ba or Y and B represents Cu or Mn. The strong on-site coulomb interaction on the d-orbital electrons of the transition metals were treated with the GGA+U approach.[9] The U_{eff} of Fe, Mn and Cu were set as 4, 3.9 and 4 eV, which were shown to give reasonable predictions of both geometric and electronic structures in previous studies.[10] To make the calculations directly comparable, we assumed a ferromagnetic (FM) state for all the cases. Previous studies indicated that magnetic ordering had relatively small effect on the oxygen vacancy formation and migration.[11] The Gibbs free energy was calculated as:

$$G = H - TS = E_{DFT} + E_{ZPE} - T(S_{vib} + S_{conf})$$

Here E_{DFT}, E_{ZPE}, S_{vib} and S_{conf} represent the DFT total energy, zero-point energy, vibrational and configurational entropy respectively. The vibrational and configurational entropy were calculated based on[12]:

$$S_{vib} = R \sum_i \left(\frac{h\nu_i/kT}{\exp\left(h\nu_i/kT\right) - 1} - \ln\left[1 - exp(-h\nu_i/kT)\right] \right)$$

$$S_{conf} = aR \cdot [\ln\left(0.5 - \delta\right) - \ln\delta]$$

where R is the ideal gas constant, h is the Plank constant, ν_i is the frequency of the ith vibrational mode, a is a factor referring to the interaction of oxygen vacancies with a=2 describing an ideal solid solution with no defect interaction. We also considered the cases when a=1 and 3, which corresponds to different extent of vacancy-vacancy interactions, but found that their impacts on the Gibbs free energies are so small (< 0.05 eV) that cannot affect our qualitative conclusions. Therefore a=2 was chosen in this study.

Selection of the base structure for DFT calculations

The phase transitions from the standard perovskite structure to brownmillerite structure was identified by the *in-situ* XRD experiments, suggesting a brownmillerite nature of doped $SrFeO_{3-\delta}$ (SF) at high temperature. To elucidate the underlying mechanism of the phase transition, First-principles simulations were carried out. Prior to detailed simulations, we carefully compared the structural differences between perovskite and brownmillerite phases of SF by redefining the lattice of SF perovskite to make their structures directly comparable (**Figure S8**). As shown in **Figure S9**, it is found that the lattice distortion is mainly caused by the ordered vacancy sites formed in brownmillerite, and these ordered oxygen vacancy sites have one-to-one correspondence with the oxygen atom sites (blue circle marked) in Perovskite. This finding can provide us guidance for the addition or removal of oxygen from brownmillerite to perovskite or perovskite to brownmillerite.
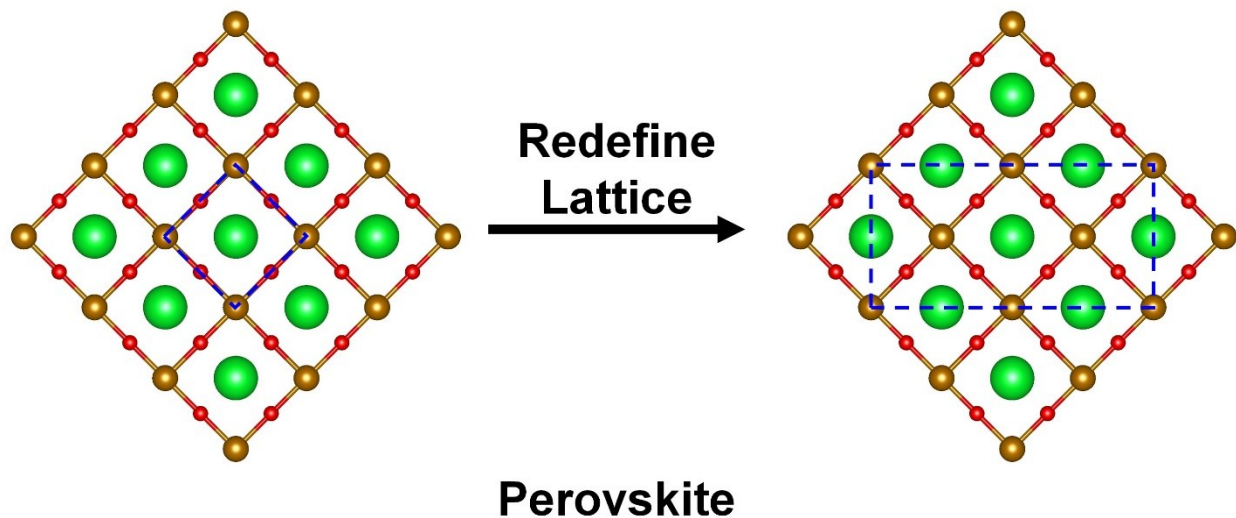
Figure S8. Reshape the lattice of perovskite with all the positions of atoms unchanged.
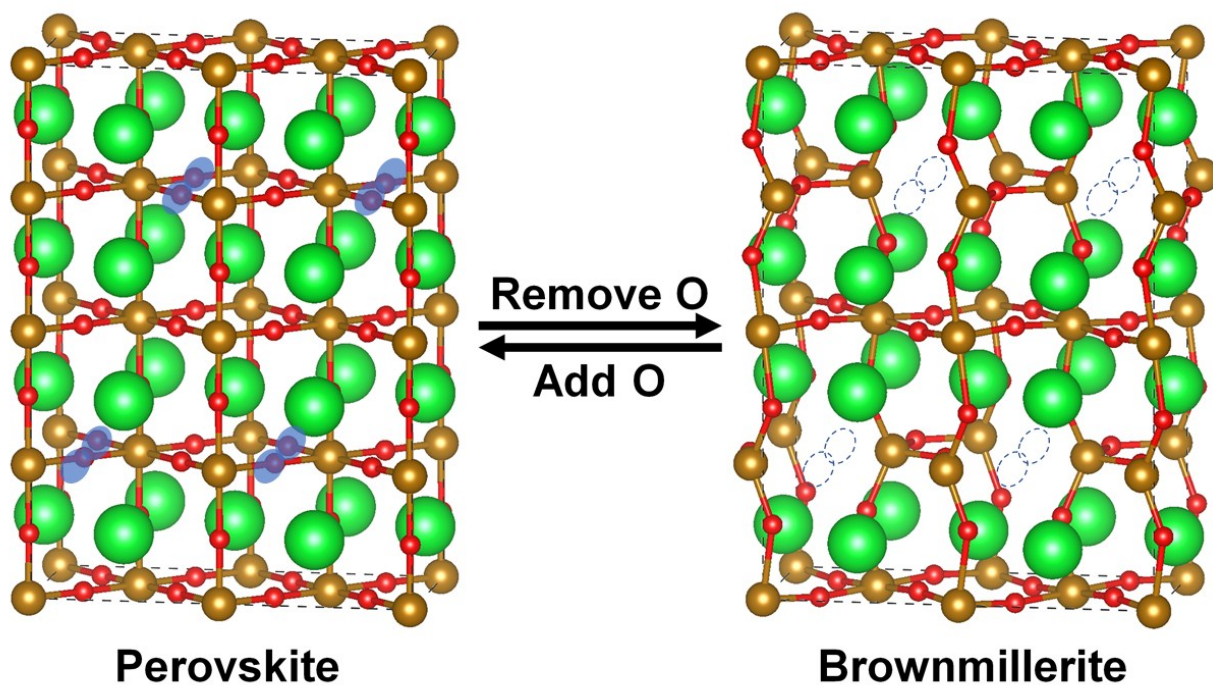
**Figure S9.** Illustration of structural differences between Perovskite and Brownmillerite.

To determine the more favorable phase at different oxygen vacancy concentration levels (δ), we calculated the Gibbs free energy of the oxides by (i) removing oxygen from the perovskite structure; and (ii) adding oxygen to the brownmillerite structure. The relative energy of the two cases at an identical oxygen vacancy concentration level would then determine the more stable form of the structure. Starting

from our $Sr_{16}Fe_{16}O_{48}$ perovskite supercell model, we removed 0, 1, 2, 3, 4 and 5 Oxygen atoms to mimic δ=0, 0.0625, 0.125, 0.1875, 0.25 and 0.3125 respectively. The removed oxygen atoms were selected from the 8 highlighted sites that correspond to the vacancy sites in brownmillerite. The 1st, 2nd, 3rd and 4th removed oxygen atoms were determined by the lowest relative energies as shown in **Figure S10**. Similarly, starting from brownmillerite, we added 4, 3, 2, 1 and 0 Oxygen atoms into the vacancy sites of the $Sr_{16}Fe_{16}O_{40}$ brownmillerite model to mimic δ=0.25, 0.3125, 0.375, 0.4375 and 0.5 respectively. The oxygen dopant sites were also determined by the lowest relative energies (**Figure S11**). To make the Gibbs free energies of all the structures with different δ comparable, all the energies were normalized by $G_\delta=G(Sr_{16}Fe_{16}O_{48-16\delta})+16\delta/2\ \mu(O_2)$. As plotted in **Figure S12**, with the increase of δ, the energies of both Perovskite and Brownmillerite models increase. Their energy intersection is located at $\delta \approx 0.26$, indicating a phase transition occurred at high temperature during the release of oxygen. Therefore, to more accurately reproduce the experimental observed δ change (usually 0.3 ~ 0.5) for all the A- and B-doped species, we would use Brownmillerite instead of Perovskite as our starting point.
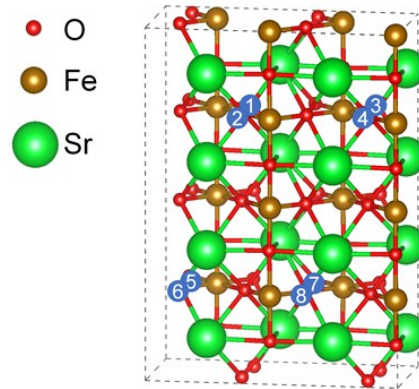
Relative Energy (eV)	1	2	3	4	5	6	7	8
1st V_O	0	0	0	0	0	0	0	0
2nd V_O	0.832	0	-	0.292	0.189	0.105	0.167	0.098
3rd V_O	0.302	-	-	0.300	0.0004	0.021	0.019	0
4th V_O	0.317	-	-	0.381	0	0.638	0.260	-
5th V_O	0	-	-	0.001	-	0.001	0.0005	-

Figure S10. Relative energies of removing 1st, 2nd, 3rd and 4th oxygen from SF Perovskite. The most stable structures (red marked) was chosen as the starting point for the removal of the next oxygen atom.
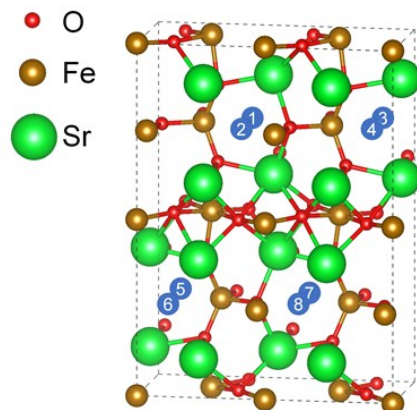
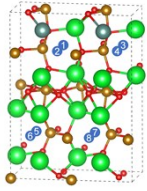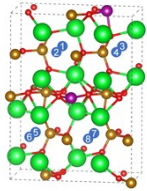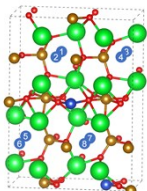| Relative Energy (eV)	1	2	3	4	5	6	7	8
1st O	0	0	0	0	0	0	0	0
2nd O	-	0.127	0.478	0	0.667	0.608	0.702	0.608
3rd O	-	0	0.00005	-	0.327	0.32813	0.355	0.355
4th O	-	-	0	-	0.265	0.360	0.310	0.336

Figure S11. Relative energies of adding 1st, 2nd, 3rd and 4th oxygen into SF Brownmillerite. The most stable structures (red marked) was chosen as the starting point for the addition of the next oxygen atom.

Using brownmillerite structures as the starting point, we explored the ΔG of vacancy formations in Ba, Y, Mn and Cu doped samples, namely A.Ba, A.Y, B.Mn and B.Cu, where A and B means A- and B-site doping. To reproduce the experimental dopant concentration (10%), we introduced 2 dopant atoms to replace the Sr or Fe atoms in our $Sr_{16}Fe_{16}O_{40}$ model, all possible non-equivalent dopant sites were tested, and the most stable ones are chosen as listed in **Table S2**. Like the way we select the added oxygen sites, all the energies of the possible sites are also listed in **Table S2**.

Table S2. Relative energies (eV) of oxygen addition in A.Ba, A.Y, B.Cu, B.Mn Brownmillerite structures.

Species \ Sites	1	2	3	4	5	6	7	8
A.Ba	0.017	0.122	0.089	0.085	0.140	2.700	0.077	0
	0.423	0.544	0.489	0.559	0.125	0.865	0	-
	0.309	0.378	0.310	0.375	0.001	0	-	-
	0.289	0.393	0.349	0.476	0	-	-	-
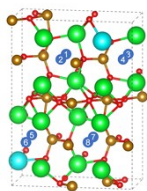
A.Y	0.478	0.503	0.374	0.388	0.113	0	0.032	0.023
	1.008	1.568	1.005	1.537	0.227	-	0	0.256
	0.675	0.748	0.670	0.744	0.009	-	-	0
	0.709	0.859	0.658	0.866	0	-	-	-
B.Mn	0.031	0.086	0.087	0.031	0.022	0.022	0	0.00003
	0.774	0.680	0.753	1.219	0.561	0	-	0.629
	0.408	0.380	0.372	0.360	0.126	-	-	0
	0.246	0.223	0.149	0.226	0	-	-	-
B.Cu	0.050	0.053	0.053	0.050	0.038	0	0.344	0.143
	0.509	0.587	0.517	0.612	0	-	0.685	0.727
	0.018	0.001	0	0.017	-	-	0.126	0.127
	0.781	0	-	0.026	-	-	0.673	0.149

Due to the limitation of the periodic boundary conditions used in our simulations, in order to more accurately simulate the possible O-O and vacancy-vacancy coupling in the experiments, a very large model is required, which would make the CPU requirements prohibitive. To estimate the error introduced by the periodic boundary conditions in our $A_{16}B_{16}O_{48-16\delta}$ Brownmillerite model, a 2× supercell mode $A_{32}B_{32}O_{82}$ model was made based on the $A_{16}B_{16}O_{41}$ model as shown in **Figure S13**. We tried to change the positions of the two added atoms in $A_{32}B_{32}O_{82}$ and found that the energy could be further lower by 1.8 eV, indicating an overestimation in the energy of $A_{16}B_{16}O_{41}$ (G(0.4375)) by 0.9 eV. Similarly, there should also be computational errors for G(0.25), G(0.3125) and G(0.375). The errors can be largely cancelled out when calculating ΔG(0.25→0.3125), ΔG(0.3125→0.375) and ΔG(0.375→4375). However, because the periodic boundary conditions would not cause error in G(0.5), the ΔG(0.4375→0.5) should be underestimated by 0.9 eV. To more accurately present the uncertainty, error bars were added in **Figure 11**. The error bars are estimated to be +0.1 eV for the upper limit and -0.3 eV for the lower limit for the first three ranges according to a previous report,[7] and -0.1 eV and +0.9 eV for the last one.
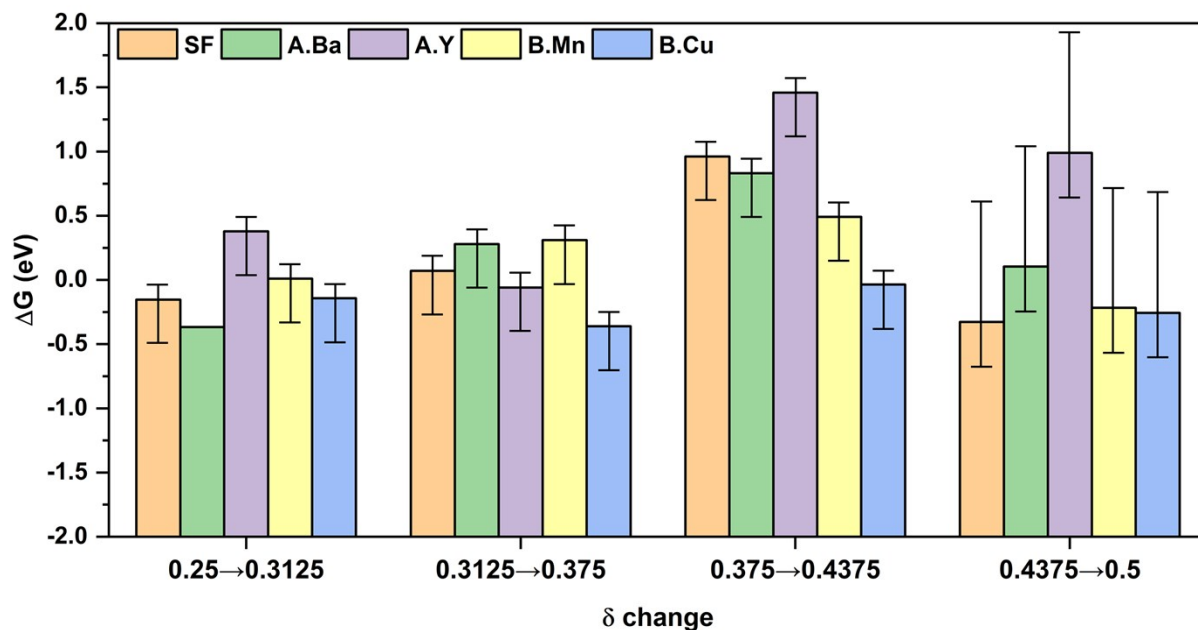
**Figure S12.** ΔG at different ranges of δ change for SF, A.Ba, A.Y, B.Mn and B.Cu at 700℃.

Brownmillerite $Sr_{32}Fe_{32}O_{80}$+2O

Side view

Top view

0 eV   -0.21   -0.94   -0.40   -1.80
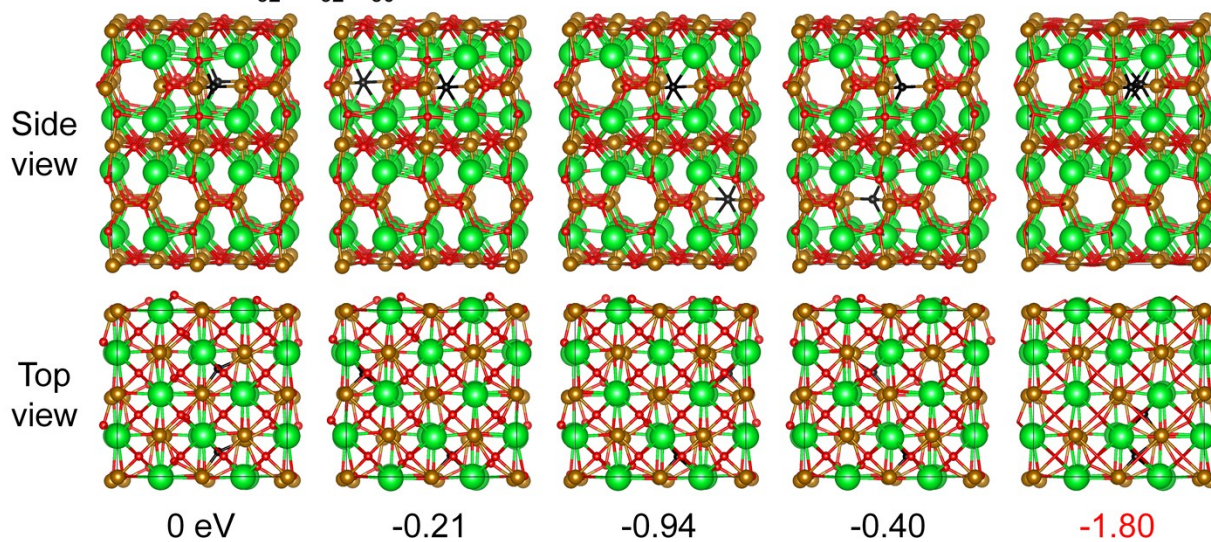
Figure S13. Relative energies of $Sr_{32}Fe_{32}O_{80}$ brownmillerite models with 2 oxygen added. The first one (reference zero point) is equivalent to a twice the size of $Sr_{16}Fe_{16}O_{40}$ considering the periodic conditions. It indicates that the neglected oxygen-oxygen interactions due to periodic conditions will overestimate the energy of the system. The error can be as large as 1.80/2=0.90 eV for the $Sr_{16}Fe_{16}O_{41}$ model we used.
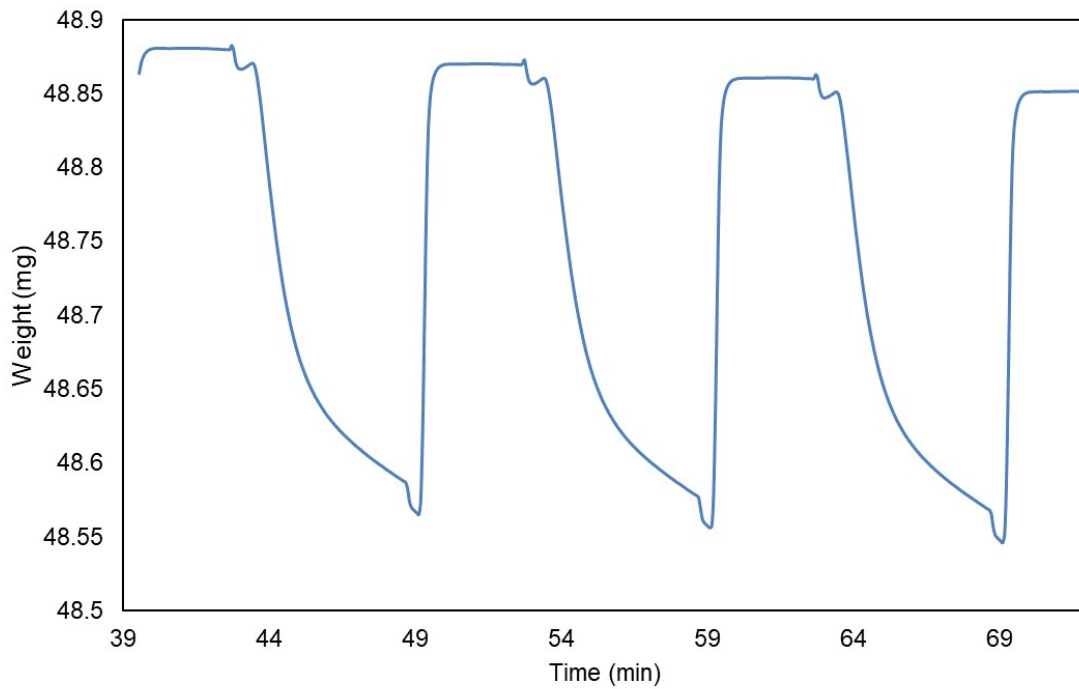
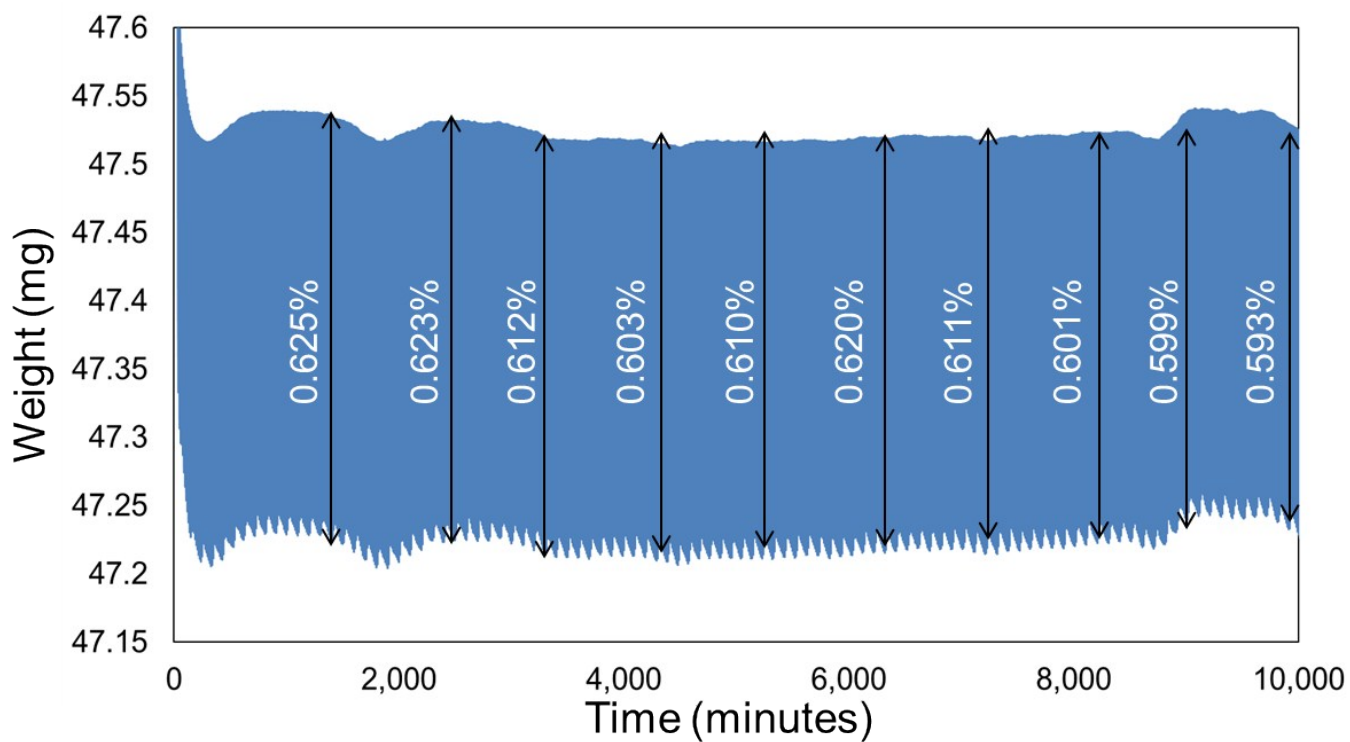**Figure S14**: Preliminary testing of $SrFe_{0.9}Mn_{0.1}O_3$ showing weight change vs time. Oxidation (in 20% O_2) was done for 4 minutes and reduction (in Ar) was done for 6 minutes.
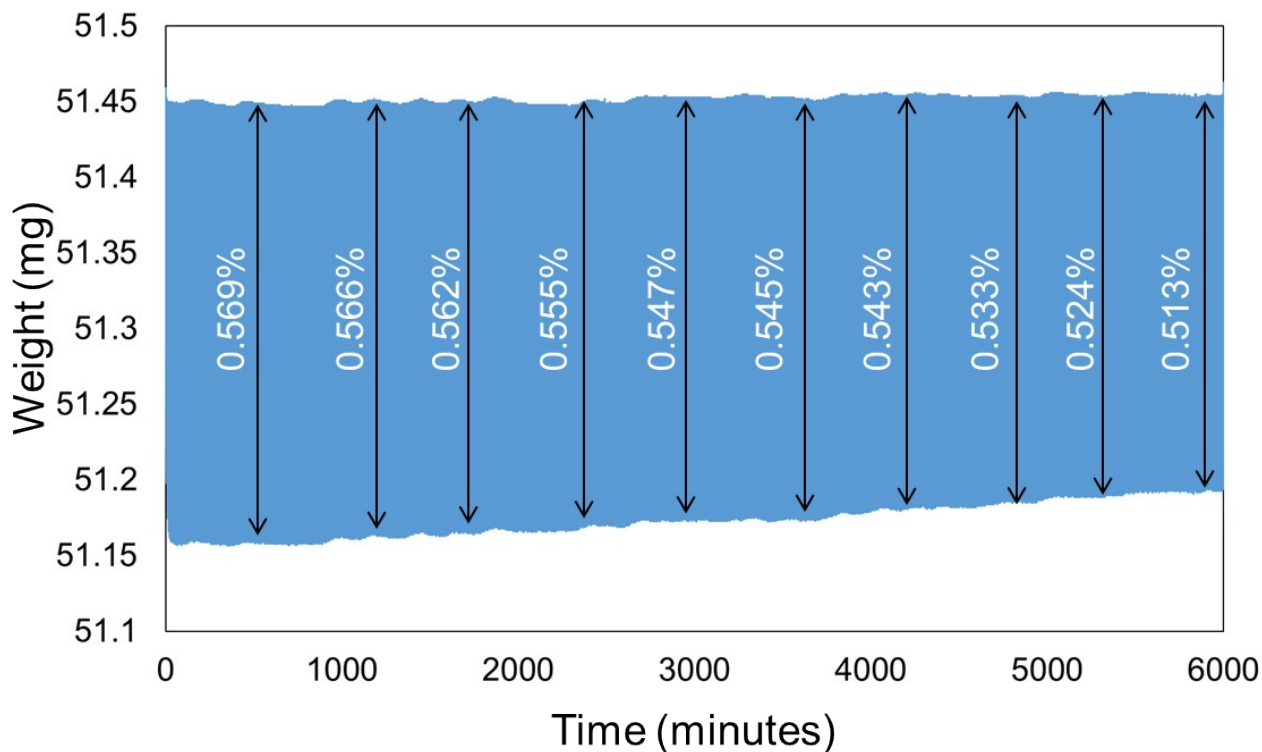
Figure S15: Long term testing of $Sr_{0.9}Ba_{0.1}FeO_3$ showing weight change vs time. Oxidation (in 20% O_2) was done for 2 minutes and reduction (in Ar) was done for 4 minutes. Arrows and percentages are displayed approximately where they were calculated from.

The average redox rate was calculated by the following equation:

$$Avg\ Redox\ Rate = \frac{(oxidation\ rate * reduction\ rate)}{(oxidation\ rate + reduction\ rate)} * 100$$
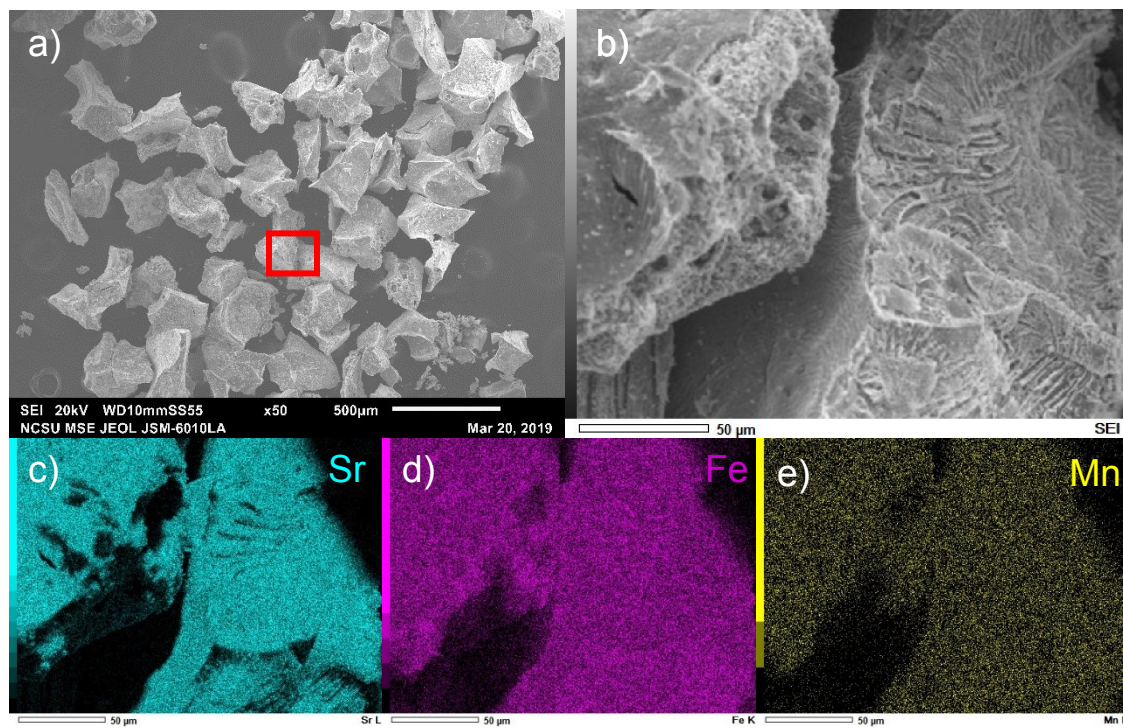
Figure S16: Long term testing of $SrFe_{0.9}Mn_{0.1}O_3$ showing weight change vs time. Oxidation (in 20% O_2) was done for 4 minutes and reduction (in Ar) was done for 6 minutes. Arrows and percentages are displayed approximately where they were calculated from.
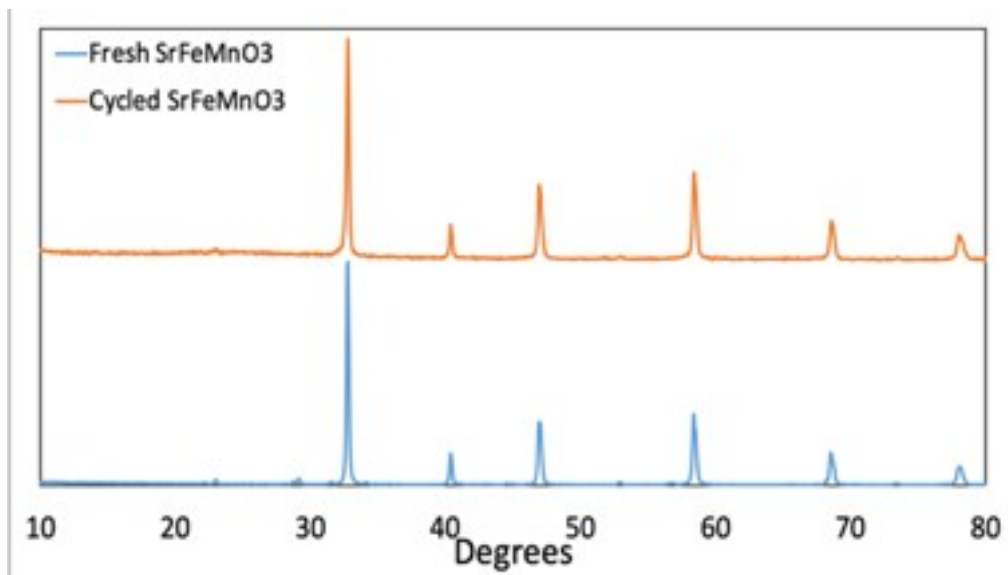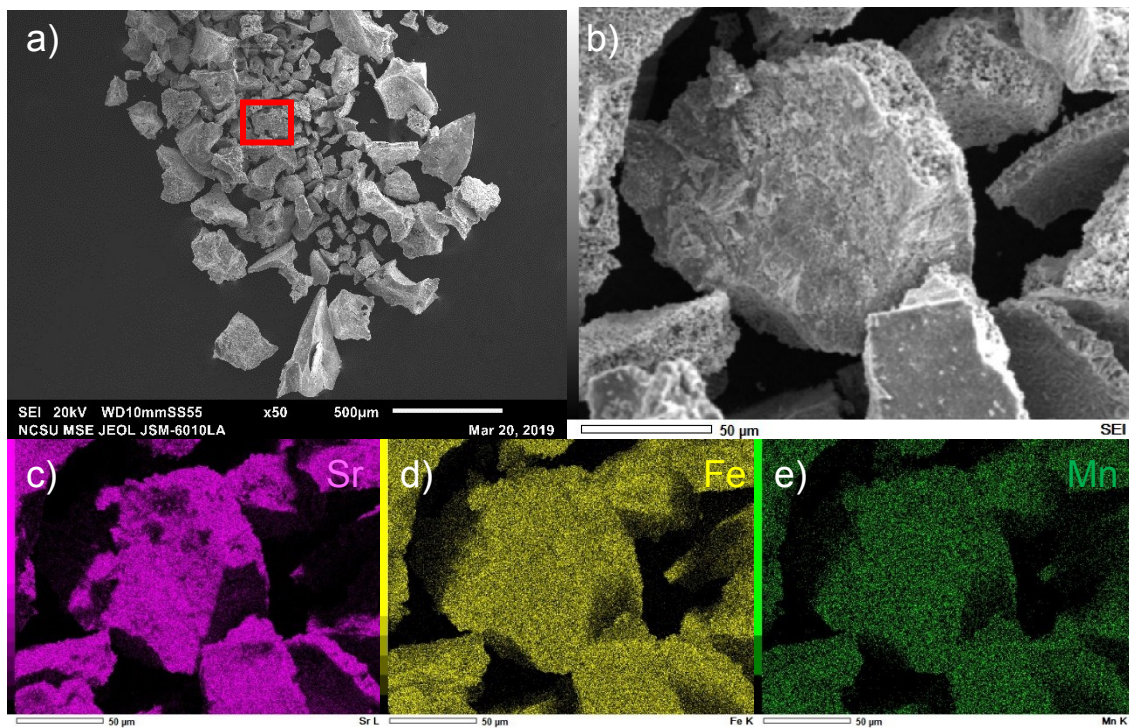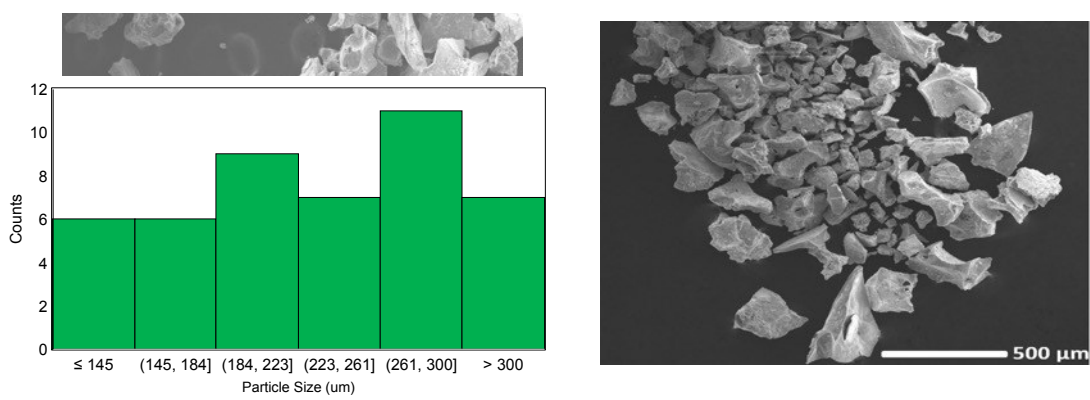
Figure S17. XRD of 1000 cycled vs fresh $SrFe_{0.9}Mn_{0.1}O_3$
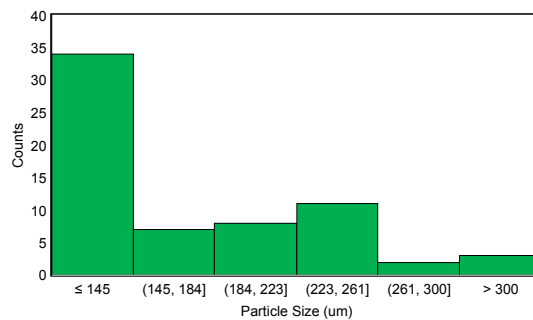
Figure S18. SEM images and (c-e) EDX mapping of $SrFe_{0.9}Mn_{0.1}O_3$ perovskite. The red rectangle in (a) marks the region of EDX mapping

Figure S19. SEM images and (c-e) EDX mapping of 1000 cycled $SrFe_{0.9}Mn_{0.1}O_3$ perovskite. The red rectangle in (a) marks the region of EDX mapping

Figure S20. (a) SEM imaging of fresh $SrFe_{0.9}Mn_{0.1}O_3$ and histogram showing particle size in um. (b) Cycled $SrFe_{0.9}Mn_{0.1}O_3$ and histogram showing particle size in um.

References

(1) I. Barin and O. Knacke; Thermochemical Properties of Inorganic Substances, 921 Pp. Springer-Verlag, Berlin, Germany, 1973.
(2) G. Pouillard, M. Shamsul Alam, M. C. Trinel-Dufour, and P. Perrot, J. Chem. Res., Synop., No. 5, 136-137 (1981).

(3)   H. S. Parker, R. S. Roth, C. D. Olson, and E. R. Plante, "NBS: Properties of Electronic Materials", Natl. Bur. Stand. (U.S.) Int. Rep., Rep. No. NBSIR 78-1483, National Bureau of Standards, U. S. Department of Commerce; Washington, D.C., Pp. 84-100 (1978).

(4)   C. L. McDaniel, National Bureau of Standards, Gaithersburg, Maryland; Private Communication.

(5)   T. Takahashi, K. Kuwabara, and Y. Kase, Denki Kagaku Oyobi Kogyo Butsuri Kagaku, 43 [5] 273-277 (1975).

(6)   Blöchl, P. E. Projector Augmented-Wave Method. *Phys. Rev. B* **1994**, *50* (24), 17953–17979. https://doi.org/10.1103/PhysRevB.50.17953.

(7)   Perdew, J. P.; Burke, K.; Ernzerhof, M. Generalized Gradient Approximation Made Simple. *Phys. Rev. Lett.* **1996**, *77* (18), 3865–3868. https://doi.org/10.1103/PhysRevLett.77.3865.

(8)   Kresse, G.; Furthmüller, J. Efficient Iterative Schemes for Ab Initio Total-Energy Calculations Using a Plane-Wave Basis Set. *Phys. Rev. B* **1996**, *54* (16), 11169–11186. https://doi.org/10.1103/PhysRevB.54.11169.

(9)   Anisimov, V. I.; Zaanen, J.; Andersen, O. K. Band Theory and Mott Insulators: Hubbard U Instead of Stoner I. *Phys. Rev. B* **1991**, *44* (3), 943–954. https://doi.org/10.1103/PhysRevB.44.943.

(10)   Hautier, Geoffroy, et al. "Accuracy of density functional theory in predicting formation energies of ternary oxides from binary oxides and its implication on phase stability." Phys. Rev. B 85.15 (2012): 155208.

(11)   Lee, Yueh-Lin, et al. "Ab initio energetics of La B O 3 (001)(B= Mn, Fe, Co, and Ni) for solid oxide fuel cell cathodes." Phys. Rev. B 85.15 (2009): 224101.

(12)   Vieten, Josua, et al. "Materials design of perovskite solid solutions for thermochemical applications." Energy & Environmental Science 12.4 (2019): 1369-1384.